



High resolution alkenone palaeobarometry indicates relatively stable $p\text{CO}_2$ during the Pliocene (3.3 to 2.8 Ma)

Journal:	<i>Philosophical Transactions A</i>
Manuscript ID:	RSTA-2013-0094
Article Type:	Research
Date Submitted by the Author:	31-Jan-2013
Complete List of Authors:	Badger, Marcus; University of Bristol, School of Earth Sciences Schmidt, D.N.; University of Bristol, School of Earth Sciences Mackensen, Andreas; Alfred Wegener Institute for Polar and Marine Research, Pancost, Richard; University of Bristol, Organic Geochemistry Unit, The Cabot Institute and Bristol Biogeochemistry Research Centre, School of Chemistry
Issue Code: Click here to find the code for your issue.:	DM1011
Subject:	Geochemistry < EARTH SCIENCES, Climatology < EARTH SCIENCES
Keywords:	Pliocene, $p\text{CO}_2$, atmospheric carbon dioxide, climate, alkenone, ODP Site 999

SCHOLARONE™
Manuscripts

1 **High resolution alkenone palaeobarometry indicates**
2 **relatively stable $p\text{CO}_2$ during the Pliocene (3.3 to 2.8**
3 **Ma)**

4 Marcus P.S. Badger^{1,2}, Daniela N. Schmidt², Andreas Mackensen³ and Richard D.
5 Pancost¹

6 ¹*Organic Geochemistry Unit, The Cabot Institute and Bristol Biogeochemistry*
7 *Research Centre, School of Chemistry, University of Bristol, Cantock's Close, Bristol,*
8 *BS8 1TS, U.K.*

9 ²*School of Earth Sciences, Bristol University, Wills Memorial Building, Queens Rd,*
10 *Bristol, BS8 1RJ, U.K.*

11 ³*Alfred Wegener Institute for Polar and Marine Research, Am Alten Hafen 26, 27568*
12 *Bremerhaven, Germany.*

13
14 **Abstract**

15 Temperature reconstructions indicate that the Pliocene was ~ 3 °C warmer globally
16 than today, and several recent reconstructions of Pliocene atmospheric CO_2 indicate
17 that it was above pre-industrial levels and similar to those likely to be seen this
18 century. However, many of these reconstructions have been of relatively low temporal
19 resolution, meaning that these records may have failed to capture variations associated
20 with the 41 Kyr glacial-interglacial cycles thought to operate in the Pliocene. Here
21 we present a new, high temporal resolution alkenone carbon isotope based record of

1
2
3 22 $p\text{CO}_2$ spanning 2.8 to 3.3 million years ago from ODP Site 999. Our record is of high
4
5 23 enough resolution (~19 Kyrs) to resolve glacial-interglacial changes beyond the
6
7 24 intrinsic uncertainty of the proxy method. The record suggests that Pliocene CO_2
8
9 25 levels were relatively stable, exhibiting variation less than 55 ppm. We perform
10
11 26 sensitivity studies to investigate the possible effect of changing sea surface
12
13 27 temperature, which highlights the importance of accurate and precise SST
14
15 28 reconstructions for alkenone palaeobarometry, but demonstrate that these
16
17 29 uncertainties do not affect our conclusions of relatively stable $p\text{CO}_2$ levels during this
18
19 30 interval.
20
21
22
23
24
25
26

27 **Keywords:** *Pliocene, $p\text{CO}_2$, atmospheric carbon dioxide, climate, alkenone, ODP*
28
29 *Site 999.*
30
31
32
33
34

35 **Introduction**

36 The Pliocene was the most recent epoch in Earth history that had global temperatures
37 greater than today; this, coupled with the similar continental positions and vegetation
38 cover to the present has led to interest in the Pliocene as a possible analogue for the
39 warmth expected by the end of the century [1]. Research to constrain the global
40 temperatures of the Pliocene has been ongoing for some time, including the
41 significant contributions of the PRISM project and successors (e.g. [2-4]), with the
42 consensus that the Pliocene was globally ~ 3 °C warmer than today. Similarly, many
43 studies suggest that Pliocene $p\text{CO}_2$ was also higher than pre-industrial levels [5-8].
44
45
46
47
48
49
50
51
52
53
54
55
56
57
58
59
60

1
2
3 44 Despite these similarities, a significant difference between the Pliocene and the
4
5 45 present day is the magnitude and pacing of Pliocene glacial-interglacial changes.
6
7 46 Based on the foraminiferal carbonate $\delta^{18}\text{O}$ record [9], Pliocene glacial-interglacial
8
9 47 cycles were less pronounced than those of the late Quaternary, and they were 41 Kyr
10
11 48 long in contrast to the 100 Kyr cycles of the last 0.7 Ma. Variations in $p\text{CO}_2$ greater
12
13 49 than the ~ 100 ppm fluctuations of the Pleistocene are, therefore, unexpected in a
14
15 50 Pliocene world, especially if, as suggested by Pagani et al. [6], Pliocene Earth-system
16
17 51 sensitivity was probably greater than 3°C for a CO_2 doubling. Consistent with this,
18
19 52 alkenone-based $p\text{CO}_2$ reconstructions have shown very little glacial-interglacial
20
21 53 variation, especially prior to the intensification of northern hemisphere glaciation at
22
23 54 2.8 Ma. These records have been, in part, confirmed by boron isotope based
24
25 55 reconstructions [7]. However, due to their low temporal resolution it is possible that
26
27 56 they fail to capture higher frequency variability in $p\text{CO}_2$ and represent neither the
28
29 57 mean state of the climate system nor its variability on glacial timescales well. A
30
31 58 recent reconstruction using boron isotopes [8] has increased the temporal resolution,
32
33 59 and in fact targeted specific glacial and interglacial peaks and troughs to attempt to
34
35 60 resolve this. Their record exhibits fluctuations in Pliocene $p\text{CO}_2$ that are in fact larger
36
37 61 (almost one and a half times) than those observed in Pleistocene ice core records [10-
38
39 62 12].
40
41
42
43
44
45

46 63 To address this apparent discrepancy, we reconstruct $p\text{CO}_2$ at similarly high
47
48 64 resolution from 3.3 to 2.8 Ma using alkenone $\delta^{13}\text{C}$ values. We apply our approach to
49
50 65 ODP Site 999 in the Caribbean because that is the same site used by Bartoli et al. [8]
51
52 66 and Seki et al. [7], allowing direct comparison of our records. Additionally, we also
53
54 67 conduct a sensitivity analysis of our reconstructed $p\text{CO}_2$ levels, allowing us to
55
56 68 constrain their potential range during this time.
57
58
59
60

1
2
3 69 **Approach and Methods**
4
5

6 70 *Alkenone palaeobarometry*
7
8

9
10 71 The isotopic fractionation between dissolved inorganic carbon and marine organic
11 72 matter during photosynthesis (ϵ_p) is controlled by, amongst other factors, the
12 73 concentration of CO_2 in the water in which the organism is photosynthesising
13 74 ($[\text{CO}_2]_{\text{aq}}$). This is ultimately controlled by the concentration of CO_2 in the overlying
14 75 atmosphere with which the ocean is in equilibrium. Other factors that can effect ϵ_p
15 76 values include physiological factors, such as cell geometry [13] and membrane
16 77 permeability [14] and environmental factors, such as nutrient and light availability
17 78 and their impact on carbon demand (i.e. growth rate) and carbon assimilation
18 79 mechanisms [15-18].
19
20

21 80 In order to constrain the physiological factors, biomarkers derived from a narrow
22 81 taxonomic range can be used rather than bulk organic matter. This approach also
23 82 prevents terrestrial or non-photosynthetically produced organic matter from biasing
24 83 the marine organic matter isotopic signature [19]. Long chain ketones (alkenones)
25 84 containing 37 carbons are produced only by a restricted group of haptophyte
26 85 organisms, such as Gephyrocapsaceae coccolithophores [20]. Thus, work over the
27 86 past 20 years has focussed specifically on the alkenone palaeobarometer as a tool to
28 87 reconstruct ancient atmospheric $p\text{CO}_2$, so long as other contributing factors (growth
29 88 rate, light regime) can be constrained. In order to determine ϵ_p values, the isotopic
30 89 composition of both the dissolved inorganic carbon pool (DIC) and organic biomass
31 90 must be known. The isotopic composition of the organic biomass ($\delta^{13}\text{C}_{\text{org}}$) is
32 91 calculated from the alkenone $\delta^{13}\text{C}$ ($\delta^{13}\text{C}_{37:2}$), corrected for a fractionation between
33
34
35
36
37
38
39
40
41
42
43
44
45
46
47
48
49
50
51
52
53
54
55
56
57
58
59
60

1
2
3 92 alkenone and haptophyte biomass by assuming a constant fractionation of 4.2 %
4
5 93 (Equation 1; [13, 16]).
6
7

8
9 Eqn. 1
$$\epsilon_{alkenone} = \frac{\delta^{13}C_{37.2} + 1000}{\delta^{13}C_{org} + 1000} - 1$$

10
11

12
13 95 The isotopic composition of DIC is estimated by measuring the $\delta^{13}C$ value of planktic
14
15 96 foraminifera, assuming the experimentally determined temperature dependent
16
17 97 fractionation between calcite and $CO_{2(g)}$ ($\epsilon_{calcite-CO_{2(g)}}$) shown in equation 2 [21]:
18
19

20
21 Eqn. 2
$$\epsilon_{calcite-CO_{2(g)}} = 11.98 - 0.12T$$

22
23

24
25 99 Where T is sea surface temperature (in degrees Celsius). This fractionation factor can
26
27 100 then be used to calculate the carbon isotopic composition of $CO_{2(g)}$ ($\delta^{13}C_{CO_{2(g)}}$):
28
29

30
31 Eqn. 3
$$\delta^{13}C_{CO_{2(g)}} = \frac{\delta^{13}C_{carbonate} + 1000}{\frac{\epsilon_{calcite-CO_{2(g)}}}{1000} + 1} - 1000$$

32
33
34

35
36 102 From this, the carbon isotopic composition of $CO_{2(aq)}$ ($\delta^{13}C_{CO_{2(aq)}}$) can be obtained
37
38 103 using the experimentally determined relationship of Mook et al., [22] as shown in
39
40 104 equations 4 and 5:
41
42

43
44 Eqn. 4
$$\epsilon_{CO_{2(aq)}-CO_{2(g)}} = \frac{-373}{T + 273.15} + 0.19$$

45
46
47

48
49 Eqn. 5
$$\delta^{13}C_{CO_{2(aq)}} = \left(\frac{\epsilon_{CO_{2(aq)}-CO_{2(g)}}}{1000} + 1 \right) \cdot (\delta^{13}C_{CO_{2(g)}} + 1000) - 1000$$

50
51
52

53 107 Photosynthetic fractionation (ϵ_p) can then be calculated from the determined
54
55 108 $\delta^{13}C_{CO_{2(aq)}}$ and $\delta^{13}C_{org}$ (equation 6):
56
57
58
59
60

1
2
3
4
5
6
7
8
9
10
11
12
13
14
15
16
17
18
19
20
21
22
23
24
25
26
27
28
29
30
31
32
33
34
35
36
37
38
39
40
41
42
43
44
45
46
47
48
49
50
51
52
53
54
55
56
57
58
59
60

109 Eqn. 6
$$\varepsilon_p = \left(\frac{\delta^{13}C_{CO_2(aq)} + 1000}{\delta^{13}C_{org} + 1000} - 1 \right) \cdot 1000$$

110 and this is then used to calculate $[CO_{2(aq)}]$ according to equation 7:

111 Eqn. 7
$$[CO_{2(aq)}] = \frac{b}{\varepsilon_f - \varepsilon_p}$$

112 where ε_f represents the isotopic fractionation during carbon fixation, assumed here to
113 be constant and 25 ‰ [16]. The 'b' term represents the summation of physiological
114 factors, such as cell size and growth rate. In the modern ocean this term shows a close
115 correlation with $[PO_4^{3-}]$, allowing estimation of 'b' by assuming past $[PO_4^{3-}]$ was
116 similar to that present at the site today (0.2 μ M; [6, 16, 23]). Finally from $[CO_{2(aq)}]$,
117 atmospheric pCO_2 can be calculated, using Henry's law (equation 8) and assuming
118 equilibrium between the surface water and overlying atmosphere:

119 Eqn. 8
$$pCO_2 = \frac{[CO_{2(aq)}]}{K_H}$$

120 The solubility coefficient (K_H) is salinity and temperature dependant, and calculated
121 following the parameterization of Weiss [24, 25]. The assumptions inherent in the
122 above treatment are discussed further below.

123 *Analytical*

124 In this study, analytical determinations of ε_p values were conducted similar to those of
125 previous alkenone paleo- pCO_2 studies (e.g. [6, 7, 23, 26-28]) from ODP Site 999
126 (12°44.639' N, 78°44.360' W, 2838 m water depth. Site 999 is slightly out of
127 equilibrium in the modern ocean, with surface waters oversaturated in CO_2 relative to
128 the atmosphere, providing a small (<10 gCm^2yr^{-1} ; [29]) net source of CO_2 to the

1
2
3 129 atmosphere. However the site has been shown to be capable of recording past changes
4
5 130 in $p\text{CO}_2$ and the air-sea equilibrium is not thought to have changed significantly from
6
7 131 the Pliocene to today (see discussion in [8]). Specifically, 27 samples were freeze
8
9 132 dried, ground by hand and solvent extracted either by Soxhlet apparatus or
10
11 133 ultrasonically. Soxhlet extractions were performed using a dichloromethane
12
13 134 (DCM):methanol (MeOH) azeotrope (2:1, v:v), refluxing for 24 hours. Ultrasonic
14
15 135 extractions were performed with, sequentially, DCM, DCM:MeOH (1:1, v:v) and
16
17 136 MeOH, repeated 3 times for each solvent with each extraction taking 15 minutes in an
18
19 137 ultrasonic bath with ~15 ml of solvent each time. Supernatants were removed and
20
21 138 combined before reduction by rotary evaporation and finally evaporated to dryness
22
23 139 under a stream of N_2 . Following elution through small (4 cm) sodium sulphate
24
25 140 columns to remove excess water, total lipid extracts were divided into apolar and
26
27 141 polar fractions using alumina flash column chromatography using 4 column volumes
28
29 142 of *n*-hexane:DCM (9:1, v:v) and 3 column volumes of MeOH, respectively. Alkenone
30
31 143 concentrations were quantified by GC-FID (Hewlett Packard 5890 Series II)
32
33 144 following trimethylsilyl derivatisation. The GC oven was programmed to increase in
34
35 145 temperature from 70°C to 130°C at 20°Cmin⁻¹, then to 300°C at 4°Cmin⁻¹, finally
36
37 146 being held isothermal for 25 min. The column was a CPSil-5CB
38
39 147 (dimethylpolysiloxane equivalent), 0.12 µm film thickness, ~50 m length and 0.32
40
41 148 mm interdal diameter with a H₂ carrier gas. Alkenone identification was confirmed by
42
43 149 GC-MS (ThermoQuest Trace MS, He carrier gas). Absolute compound concentrations
44
45 150 were quantified by reference to an internal standard (hexadecan-2-ol) added prior to
46
47 151 column chromatography.
48
49
50
51
52
53
54
55 152 Sea surface temperature (SST) was reconstructed using the alkenone unsaturation
56
57 153 index ($U_{37}^{K'}$; [30, 31]; equation 9):
58
59
60

1
2
3 154 Eqn. 9 $U_{37}^{K'} = [C_{37:2}] / [C_{37:2} + C_{37:3}]$
4
5

6
7 155 Where $C_{37:2}$ is the di-unsaturated methyl alkenone and $C_{37:3}$ is the tri-unsaturated
8
9 156 compound. SSTs were then calculated using the calibration of Müller et al. [32]
10
11 157 (equation 10):
12

13
14 158 Eqn. 10 $U_{37}^{K'} = 0.033T + 0.044$
15
16

17
18 159 Concerns have been raised about the use of $U_{37}^{K'}$ as the index approaches 1 [33]. This
19
20 160 would be of particular concern at Site 999 as over the studied interval $U_{37}^{K'}$ is > 0.9 .
21
22

23 161 However the challenge of calibrating SSTs towards the upper limit of $U_{37}^{K'}$ seems to
24
25 162 be a problem largely restricted to sediment trap based calibrations. For core tops a
26
27 163 linear calibration seems to hold true, and in fact the updated core-top calibration of
28
29 164 Conte et al., [33] is essentially identical to that of Muller et al., [32] (which is more
30
31 165 widely used and therefore our preferred). They are especially similar towards the top
32
33 166 end of the scale. As we are dealing here with alkenones which have made it to the sea
34
35 167 floor a core top calibration seems most appropriate.
36
37

38
39 168 Alkenone isotope analyses were performed on a ThermoFisher Delta V connected via
40
41 169 a GC isolink and conflo IV to a Trace GC. The GC oven was programmed to increase
42
43 170 in temperature from 70°C to 200°C at 20°Cmin⁻¹ then to 300°C at 6°Cmin⁻¹ and
44
45 171 finally held isothermal for 25 min. Conversion to the VPDB scale was calculated by
46
47 172 reference to a laboratory standard gas tank of known $\delta^{13}\text{C}$. Instrument performance
48
49 173 was monitored using an in house fatty acid methyl ester standard and long term
50
51 174 precision is ~0.3 %.
52
53
54
55
56
57
58
59
60

1
2
3 175 Ten to fifteen specimens of the planktic foraminifera *Globigerinoides ruber* were
4
5 176 picked from the 300-350 μm fraction for $\delta^{13}\text{C}$ analysis. This was determined with a
6
7 177 Finnigan MAT 251 with an online automatic carbonate preparation device at the
8
9 178 Alfred Wegener Institute for Polar and Marine Research, Bremerhaven. Calibration to
10
11 179 the VPDB scale was performed using the international NBS19 standard.
12
13 180 Reproducibility is better than ± 0.06 ‰ over a one-year period based on repeat
14
15 181 measurements of a laboratory standard.
16
17

18
19 182 The age model for ODP Site 999 is as discussed in Seki et al. [7]. Uncertainty
20
21 183 propagation on our alkenone-derived CO_2 estimates was performed by Monte Carlo
22
23 184 modelling ($n=25000$). Uncertainties of 2 °C and 0.1 ‰ were applied to temperature
24
25 185 and foraminiferal calcite $\delta^{13}\text{C}$, (normal probability function (pdf), 2 σ error) and 2 and
26
27 186 0.1 to salinity and $[\text{PO}_4^{3-}]$, respectively (2 σ ; uniform pdf). 2 σ errors on alkenone $\delta^{13}\text{C}$
28
29 187 were estimated from replicate runs, calcite $\delta^{13}\text{C}$ from repeat runs of an internal
30
31 188 standard, estimated integrated analytical and calibration error for $U_{37}^{K'}$ based
32
33 189 temperatures [32] and conservative estimates of likely variation for salinity and $[\text{PO}_4^{3-}]$.
34
35 190]. An 11 % error on the slope of $b=a[\text{PO}_4]+c$ was assumed [26].
36
37
38
39
40
41

42 **Results**

43
44
45 192 Alkenone and *G. ruber* $\delta^{13}\text{C}$ values (Figure 1b) were used to calculate ε_p values
46
47 193 (Figure 1a). These ε_p values are fairly stable throughout the study interval, varying
48
49 194 between 12.2 and 9.4 ‰. This is close to the values reported by Seki et al., [7] for the
50
51 195 same Site over this interval (12.2 - 10.9 ‰).
52
53

54
55 196 Using modern $[\text{PO}_4^{3-}]$ for the Caribbean Sea, ε_p values can be converted to $[\text{CO}_2]_{(\text{aq})}$
56
57 197 (Equation 7; Figure 1b). Using our SSTs derived from $U_{37}^{K'}$ indices and assuming air-

1
2
3 198 sea equilibrium, $[\text{CO}_2]_{(\text{aq})}$ can then be used to determine atmospheric $p\text{CO}_2$ (Equation
4
5 199 8). $U_{37}^{K'}$ indices range from 0.90 to 0.99 (close to the maximum recordable value for
6
7
8 200 $U_{37}^{K'}$), resulting in SSTs at Site 999 of $\sim 28^\circ\text{C}$ that show a slight decrease over the 500
9
10
11 201 Kyrs of our record (Figure 2b). These are $\sim 2^\circ\text{C}$ higher than the planktic foraminifer
12
13 202 (*Globigerinoides sacculifer*) Mg/Ca based SST record of Groeneveld [34] from the
14
15 203 same site, $< 1^\circ\text{C}$ lower than the SSTs estimated by Bartoli et al. [8] based on a
16
17 204 seawater Mg/Ca correction of these same data, and very similar to modern SSTs that
18
19 205 range from 26.7°C to 28.2°C [35].

20
21
22 206 Our resulting $p\text{CO}_2$ reconstruction (Figure 2a) reveals relatively stable $p\text{CO}_2$ values
23
24 207 that are within the range of previously published alkenone records from ODP Site 999
25
26
27 208 (without the lith size correction of Seki et al. [7]) and elsewhere [6]. All of our
28
29 209 reconstructed $p\text{CO}_2$ (250-300 ppm) levels are similar to or slightly higher than the
30
31 210 240-290 ppm for Pleistocene interglacials reconstructed from ice cores [10-12] and
32
33 211 are consistent with glacial-interglacial variability of at most 40 ppm. In fact, the entire
34
35 212 range of determined $p\text{CO}_2$ values for the end of the Pliocene is less than the 80 ppm
36
37 213 difference between the Holocene and the Last Glacial Maximum [36]. There is some
38
39 214 variability outside of uncertainty in the ε_p record in the younger part of the record,
40
41 215 hinting to some variability after 3 Ma, however once the full propagation of
42
43 216 uncertainties are taken through to the CO_2 reconstruction, the variation is no longer
44
45 217 significant. Below, we discuss the $p\text{CO}_2$ estimates, their variations with respect to
46
47 218 Pliocene glacial-interglacial cycles and the potential range of $p\text{CO}_2$ given our
48
49 219 assumptions of growth rate and SST.
50
51
52
53
54
55 220

56 57 58 221 **Discussion**

59
60

222 *Glacial-Interglacial pCO₂ variations*

223 We estimate absolute *p*CO₂ to be around ~270 ppm for much of the period studied
224 here, based on our most likely temperature, cell geometry and growth rates
225 assumptions (see subsequent sections for sensitivity analysis of these parameters).
226 This is similar to pre-industrial levels, and around the peak level of the Pleistocene ice
227 core records (298.6 ppm; [10-12]). Our record is within the range of estimates given
228 by Pagani et al., [6] (Figure 3a), although it should be noted that these authors report a
229 broad range of absolute CO₂ due to differences between the sites. Our record is below
230 the ‘CO_{2slope}’ reported in Pagani et al. [6] i.e. their extrapolated trend from the early
231 Pliocene to the present day.

232 Estimating absolute *p*CO₂ from a single site is complicated by uncertainty as to
233 whether the site has been in equilibrium with the atmosphere over the period of
234 interest. As highlighted by Pagani et al. [6], different sites can exhibit very different
235 estimates for atmospheric *p*CO₂, as not all of the surface ocean is in equilibrium with
236 the atmosphere [29]. The surface ocean at Site 999 is close to equilibrium today [29]
237 and reconstructed alkenone based *p*CO₂ values are similar to ice core records where
238 they overlap in the Pleistocene [7] suggesting that the site was in equilibrium through
239 much of this time. It is difficult to know whether this remained so in the Pliocene with
240 different circulation in the Caribbean, so as with all single site records, our absolute
241 *p*CO₂ should be treated with some care.

242 Our absolute *p*CO₂ is similar to the alkenone-based record without secondary
243 corrections of Seki et al. [7] from the same site, although somewhat lower than both
244 the cell size corrected alkenone record and boron isotope based records of Seki et al.
245 [7] (Figure 3a). Bartoli et al. [8] report a broad range of *p*CO₂ (170-400 ppm; Figure

1
2
3 246 3b) and our record is within that range. The difference between our record and the
4
5 247 cell size corrected record of Seki et al. [7] (Figure 4) highlights the importance of
6
7 248 secondary corrections, particularly on alkenone based method and we explore this
8
9 249 further below. Given the potential difficulty of assessing absolute $p\text{CO}_2$ levels from
10
11 250 single site records we now focus on $p\text{CO}_2$ variability during this interval in the
12
13 251 Pliocene.

14
15
16
17 252 Previous alkenone-based palaeobarometry has been at a relatively low temporal
18
19 253 resolution, and given the 41 kyr glacial-interglacial variability in the Pliocene world,
20
21 254 it is possible that these records do not capture rapid changes in $p\text{CO}_2$ [6, 7]. Our new
22
23 255 record increases the resolution of the alkenone-based records, but unlike the boron
24
25 256 record of Bartioli et al. [8] shows virtually invariant $p\text{CO}_2$ within the precision of the
26
27 257 alkenone palaeobarometer (Figure 4). The differences between these two records
28
29 258 cannot be due to differences in ocean-atmosphere equilibrium, as both are based on
30
31 259 Site 999. The magnitude of variability in our record is similar to that seen in previous,
32
33 260 low resolution records (i.e. the boron and alkenone records of Seki et al. [7], and the
34
35 261 alkenone records of Pagani et al. [6]) which may suggest that these records have
36
37 262 captured $p\text{CO}_2$ variability despite their lower resolution, and the small estimated range
38
39 263 of Pliocene $p\text{CO}_2$ is a feature of Pliocene climate dynamics rather than a sampling
40
41 264 artefact. An alternative hypothesis is that the alkenone palaeobarometer
42
43 265 underestimates variability for an as yet unknown reason.

44
45
46
47
48
49 266 It should perhaps not be surprising that Pliocene $p\text{CO}_2$ appears to be relatively stable;
50
51 267 the large, 100 Kyr glacial-interglacial cycles of the Pleistocene are associated with ~
52
53 268 100 ppm of change in $p\text{CO}_2$ [10-12], and it is likely that the smaller amplitude
54
55 269 variations in the Pliocene would be associated with significantly smaller $p\text{CO}_2$
56
57
58
59
60

1
2
3 270 changes. The large amplitude changes of Bartoli et al. [8] are therefore somewhat
4
5 271 surprising. Given that the full uncertainty envelope for our alkenone $p\text{CO}_2$ records is
6
7 272 approximately ± 40 ppm, it is plausible that smaller, Pliocene variations in $p\text{CO}_2$
8
9 273 would be below the detection limit of our methods.
10

11
12
13 274

14
15
16 275 *Cell size and productivity corrections*
17

18
19 276 Atmospheric $p\text{CO}_2$ reconstructions from alkenone isotopes can be affected by cell
20
21 277 size and productivity, i.e growth rate variations. Seki et al. [7] applied a conceptual
22
23 278 cell size correction to the alkenone data from Site 999, based on the low resolution
24
25 279 lith size record of Kameo and Bralower [37]. However, recent high resolution data
26
27 280 shows no evidence of changes in coccolith size over the time interval of interest [38].
28
29 281 Crucially, there are no changes in coccolith size – and thus, inferred coccolithophorid
30
31 282 cell size – on glacial-interglacial timescales, and hence it is unlikely that they could
32
33 283 account for the low variability observed here. It remains possible, however, that they
34
35 284 could account for the relatively low absolute $p\text{CO}_2$ values determined for the Pliocene
36
37 285 at Site 999, compared to $\delta^{11}\text{B}$ -based estimates (~ 400 ppm; [7, 8]).
38
39
40
41

42 286 There is not yet a consensus approach to the application of a cell geometry correction
43
44 287 (see discussion in Seki et al. [7] and Henderiks and Pagani [39]), however attempts
45
46 288 have been made to correct for cell size changes by adjusting the ‘ b ’ term in equation
47
48 289 7. Hendericks and Pagani [39] adjusted the ‘ b ’ term based on the ratio of “fossil”
49
50 290 haptophyte cell volume:surface area ($V:SA_{fossil}$) to that of the modern *Emiliania*
51
52 291 *huxleyi* ($V:SA_{E.hux}$) used for modern culture studies. (equation 11).
53
54
55
56
57
58
59
60

1
2
3
4
5
6
7
8
9
10
11
12
13
14
15
16
17
18
19
20
21
22
23
24
25
26
27
28
29
30
31
32
33
34
35
36
37
38
39
40
41
42
43
44
45
46
47
48
49
50
51
52
53
54
55
56
57
58
59
60

292 Eqn. 11
$$b' = b \cdot \left[\frac{V : SA_{fossil}}{V : SA_{E.hux}} \right]$$

293 Popp et al., 1998 determined $V:SA_{E.hux}$ to be $0.9 \pm 0.1 \mu\text{m}$ and the value of $V:SA_{fossil}$
294 can be estimated using the relationship between cell diameter (D_{cell}) and
295 *Reticulofenestra* coccolith length ($L_{coccolith}$; [39]; equation 12):

296 Eqn. 12
$$D_{cell} = 0.55 + 0.88 \cdot L_{coccolith}$$

297 Reticulofenestrids (Noelaerhabdaceae) are thought to be important alkenone
298 producers in the past [39], although there is some evidence that this may not be the
299 case for some earlier parts of the Neogene [40].

300 The cell size correction results in a linear correction to $p\text{CO}_2$, the gradient of which is
301 temperature dependent (Figure 5), where a larger coccolith length results in higher
302 reconstructed CO_2 . This effect is increased at higher SSTs. Approximately $1 \mu\text{m}$ of
303 change in $L_{coccolith}$ would be required to alter $p\text{CO}_2$ beyond our uncertainty envelope.
304 This represents a size change of $\sim 25\%$, and there is no evidence for such a change on
305 glacial-interglacial timescales at Site 999 [38].

306 Similarly, there is no evidence that growth rate changed on glacial-interglacial
307 timescales at Site 999 through the interval studied. Seki et al. [7] noted that there
308 could have been changes in the oceanography of the site as the shoaling of the
309 Panama isthmus isolated the Caribbean from the Pacific. O'Dea et al. [41] had argued
310 that these changes could have influenced the nutrient regime at Site 999; however, the
311 closure of the strait to deep water is thought to have been complete by 4.6 Ma [42].
312 Moreover, alkenone and other biomarker concentrations and mass accumulation rates
313 are low and relatively invariant over the studied interval [7]. Other indicators of

1
2
3 314 productivity (organic carbon mass accumulation rates) have not shown evidence of
4
5 315 significant changes in productivity [43]. We have improved the resolution of these
6
7 316 analyses to 16-kyr and no systematic variation is apparent, suggesting that on glacial-
8
9 317 interglacial timescales no correction to our $p\text{CO}_2$ reconstruction is justified.

10
11
12 318 No proxy exists to directly reconstruct the growth rate conditions at the site during the
13
14 319 Pliocene. Our approach is to use the relationship between 'b' and $[\text{PO}_4^{3-}]$ which has
15
16 320 been calibrated globally [6, 23, 44] and appears to be a proxy for growth limiting
17
18 321 nutrients [23]. Our favoured assumption is to use a modern day value for surface
19
20 322 water $[\text{PO}_4^{3-}]$ at Site 999 [45] but here we explore the possibility that this assumption
21
22 323 is incorrect. To this end, we have performed a sensitivity test, and apply a $[\text{PO}_4^{3-}]$
23
24 324 which represents an oligotrophic site ($0.05 \mu\text{M}$), a high nutrient area similar to present
25
26 325 day eastern equatorial Pacific ($0.6 \mu\text{M}$) and an extreme case representative of an
27
28 326 active upwelling region ($0.9 \mu\text{M}$)[45]. The resulting $p\text{CO}_2$ reconstructions vary from
29
30 327 ~ 230 ppm for the oligotrophic model, ~ 390 ppm for the eastern equatorial pacific
31
32 328 model, and ~ 480 ppm for the extreme case (Figure 6). The sensitivity tests
33
34 329 demonstrate that our favoured assumptions that result in $p\text{CO}_2$ of ~ 270 ppm may be a
35
36 330 lower bound, and if the nutrient regime was significantly different in the Pliocene then
37
38 331 our record may be an underestimate. However, as discussed above, we have no direct
39
40 332 evidence for such a change, and critically, no evidence of changes on glacial-
41
42 333 interglacial timescales that may explain the low variability of our record.
43
44
45
46
47
48

49 334

50
51
52 335 *The importance of accurate and precise temperature determinations*

53
54
55 336 Critical to the validity of alkenone isotope $p\text{CO}_2$ reconstructions is the accurate and
56
57 337 precise determination of sea surface temperature. Whilst some of the previously
58
59
60

1
2
3 338 discussed parameters (such as an evolutionary change in haptophyte cell size, or
4
5 339 significant changes in oceanographic regime leading to changes in growth rate) are
6
7 340 likely stable over short periods of time, sea surface temperatures can change on
8
9 341 glacial-interglacial timescales and affect $p\text{CO}_2$ estimates. SST is involved three times
10
11 342 in the reconstruction of $p\text{CO}_2$ from alkenone $\delta^{13}\text{C}$ values, in the conversion of
12
13 343 $\delta^{13}\text{C}_{\text{calcite}}$ to $\delta^{13}\text{C}_{\text{CO}_2(\text{g})}$ values (equations 2 - 3), $\delta^{13}\text{C}_{\text{CO}_2(\text{g})}$ to $\delta^{13}\text{C}_{\text{CO}_2(\text{aq})}$ values
14
15 344 (equations 4 -5) and the calculation of the solubility coefficient (equation 8). This
16
17 345 results in a non-linear temperature dependence of the $\delta^{13}\text{C}_{\text{alkenone}}-p\text{CO}_2$ relationship
18
19 346 (Figure 7). The size of this effect can be important both in terms of accuracy and
20
21 347 precision of alkenone-based reconstructions. Proxies that show potential to
22
23 348 reconstruct SST suitable for alkenone palaeobarometry include those based on
24
25 349 alkenone unsaturation indices [30, 31] and planktic foraminiferal Mg/Ca ratios [46].
26
27 350 Estimates of uncertainty in the measurement of SST using either Mg/Ca or alkenone
28
29 351 unsaturation suggests a combined analytical and correlation error of approximately 2
30
31 352 $^{\circ}\text{C}$ (2σ ; [47, 48]),

32
33
34
35
36
37 353 The relationships between alkenone $\delta^{13}\text{C}$, ε_p , $[\text{CO}_2]_{(\text{aq})}$ and $p\text{CO}_2$, and the effects of
38
39 354 SST are shown in Figure 7. Higher reconstructed SST results in higher apparent ε_p for
40
41 355 a given $\delta^{13}\text{C}$ value (Figure 7a) and higher $p\text{CO}_2$ for a given $[\text{CO}_2]_{(\text{aq})}$ (Figure 7b).
42
43 356 Higher reconstructed SST, therefore, results in higher apparent $p\text{CO}_2$ for a given $\delta^{13}\text{C}$
44
45 357 value by integrating these two effects (Figure 7d). The magnitude of this effect is
46
47 358 more pronounced at higher $p\text{CO}_2$ and more negative alkenone $\delta^{13}\text{C}$ values (Figure
48
49 359 7d), and also as ε_p approaches ε_f (see the discussion in Pagani et al. [27]).
50
51
52

53
54 360 For example, for an alkenone $\delta^{13}\text{C}$ value of -25 ‰ (which gives a representative $p\text{CO}_2$
55
56 361 of 300 ppm in this sensitivity test), the 2 $^{\circ}\text{C}$ analytical and calibration error in Mg/Ca
57
58
59
60

1
2
3 362 or $U_{37}^{K'}$ SST estimates would result in a error of ~ 23 ppm in $p\text{CO}_2$; at a more negative
4
5 363 $\delta^{13}\text{C}$ value of -28 ‰ ($p\text{CO}_2=400$ ppm) the same error in SST results in an error of ~ 34
6
7 364 ppm in $p\text{CO}_2$ (Figure 7d). One result of this is that an incorrect or overestimated
8
9
10 365 decline in SST can lead to an artificial apparent decline in $p\text{CO}_2$. This requires careful
11
12 366 consideration if estimating climate or earth system sensitivity from coupled alkenone
13
14 367 $p\text{CO}_2$ and SST records. To apply this directly to the data presented here, SSTs 2 °C
15
16 368 cooler than our data suggests (ie at the edge of the quoted uncertainty for alkenone
17
18 369 unsaturation based temperatures) would result in average reconstructed $p\text{CO}_2$ over the
19
20 370 interval studied of 255 ppm, a 15 ppm reduction. Conversely SSTs 2 °C warmer
21
22
23 371 would give average reconstructed $p\text{CO}_2$ 20 ppm higher, at 290 ppm.
24
25
26
27
28
29

30 373 For the Pliocene, the choice of SST record is important, given the uncertainty as to the
31
32 374 possible effects of changing $\text{Mg}/\text{Ca}_{\text{sw}}$ on Mg/Ca palaeothermometry. Recent
33
34 375 reconstructions of Pliocene $\text{Mg}/\text{Ca}_{\text{sw}}$ suggest that the Pliocene value could have been
35
36 376 more than 1 mol/mol lower [49], which could change the reconstructed SST by as
37
38 377 much as 6 °C . Our preferred $U_{37}^{K'}$ temperatures for Site 999 lie between the $\text{Mg}/\text{Ca}_{\text{sw}}$
39
40
41 378 corrected and uncorrected records for the same time period [8, 34]. The uncorrected
42
43 379 SST estimates of Groeneveld [34] are ~ 3.8 °C lower and would result in $p\text{CO}_2 \sim 29$
44
45 380 ppm lower if applied to our records, whereas the up to 2.5 °C higher temperatures of
46
47
48 381 Bartoli et al. [8] would increase our estimates by ~ 24 ppm. At Site 999 today SSTs
49
50 382 vary between 26.7 °C and 28.2 °C whereas temperatures at the habitat depth likely for
51
52 383 *G. sacculifer* it is $24.2 - 26.6$ °C [35], and so the cooler temperatures of Groeneveld
53
54 384 [34] may be due to differences in depths of the recording organism. Crucially
55
56
57 385 however, none of the SST records for Site 999 indicate glacial – interglacial
58
59
60

1
2
3 386 variability that would result in $p\text{CO}_2$ variations with a magnitude similar to those of
4
5 387 the Pleistocene, or as recorded by Bartoli et al., [8].
6
7

8 388
9

11 389 **Synthesis**

12
13
14 390 We reconstruct atmospheric $p\text{CO}_2$ for the Pliocene (3.3 to 2.8 Ma) of $\sim 270 \pm 40$ ppm
15
16
17 391 (2σ) similar to Pleistocene interglacials. We record little or no variability suggesting
18
19 392 $p\text{CO}_2$ was persistently at about Pleistocene interglacial values. Only at the outer
20
21 393 bounds of our uncertainty envelope would we record Pleistocene glacial levels of
22
23 394 $p\text{CO}_2$. Uncertainty in our assumptions for productivity, SST and cell size all result in
24
25 395 a broad uncertainty envelope around our preferred parameterization, with our best
26
27 396 estimate suggesting $p\text{CO}_2$ was between ~ 230 and 300 ppm. These absolute values are
28
29 397 lower than those derived from other approaches and this could reflect a combination
30
31 398 of local paleoceanographic conditions and the impact of secondary effects on
32
33 399 alkenone $\delta^{13}\text{C}$ values. However, we see no evidence that such secondary effects were
34
35 400 varying on glacial-interglacial timescales, and consequently, our data collectively
36
37 401 indicate that $p\text{CO}_2$ at this point in the Pliocene was relatively stable. We see no
38
39 402 evidence for glacial-interglacial changes larger than the fundamental precision of the
40
41 403 proxy method of 40 ppm, and our record supports the idea that minimal $p\text{CO}_2$
42
43 404 variability was associated with the small glacial-interglacial climate variability of the
44
45 405 Pliocene. However, further work is needed to improve the precision of all proxy
46
47 406 methods, and to reconcile differences between records of Pliocene $p\text{CO}_2$.
48
49
50
51
52

53 407
54

56 408 **Acknowledgments**

57
58
59
60

1
2
3 409 This research used samples and data provided by the Ocean Drilling Program which is
4
5 410 sponsored by the U.S. National Science Foundation and participating countries under
6
7 411 the management of Joint Oceanic Institutions. We would like to thank Alex Hull,
8
9 412 Gemma Bowler and Marilyn Potts for labwork, Lisa Schönborn and Günter Meyer for
10
11 413 technical assistance and Alison Kuhl and Ian Bull of the NERC Life Sciences Mass
12
13 414 Spectrometry facility for research support. We thank two anonymous reviewers and
14
15 415 the editor, Dan Lunt, for careful comments which greatly improved the manuscript.
16
17 416 MPSB was funded by NERC grant NE/H006273/1, DNS by a Royal Society URF.
18
19 417 RDP acknowledges the Royal Society Wolfson Research Merit Award.
20
21
22
23

24 418 **References**

- 25
26
27 419 1. Solomon, S., et al., *Contribution of Working Group I to the Fourth Assessment*
28 420 *Report of the Intergovernmental Panel on Climate Change 2007*, Cambridge,
29 421 U.K. and New York, USA: Cambridge University Press.
30 422 2. Dowsett, H., J. Barron, and R. Poore, *Middle Pliocene sea surface*
31 423 *temperatures: A global reconstruction*. *Marine Micropaleontology*, 1996.
32 424 **27**(1-4): p. 13-25.
33 425 3. Dowsett, H.J., *The PRISM palaeoclimate reconstruction and Pliocene sea-*
34 426 *surface temperature*. *Deep-Time Perspectives on Climate Change: Marrying*
35 427 *the Signal from Computer Models and Biological Proxies*, ed.
36 428 M.H.A.M.G.F.J.S.D.N. Williams 2007. 459-480.
37 429 4. Dowsett, H.J., et al., *Sea surface temperatures of the mid-Piacenzian Warm*
38 430 *Period: A comparison of PRISM3 and HadCM3*. *Palaeogeography*
39 431 *Palaeoclimatology Palaeoecology*, 2011. **309**(1-2): p. 83-91.
40 432 5. Raymo, M.E., et al., *Mid-Pliocene warmth: Stronger greenhouse and stronger*
41 433 *conveyor*. *Marine Micropaleontology*, 1996. **27**(1-4): p. 313-326.
42 434 6. Pagani, M., et al., *High Earth-system climate sensitivity determined from*
43 435 *Pliocene carbon dioxide concentrations*. *Nature Geoscience*, 2010. **3**(1): p. 27-
44 436 30.
45 437 7. Seki, O., et al., *Alkenone and boron-based Pliocene pCO₂ records*. *Earth and*
46 438 *Planetary Science Letters*, 2010. **292**(1-2): p. 201-211.
47 439 8. Bartoli, G., B. Honisch, and R.E. Zeebe, *Atmospheric CO₂ decline during*
48 440 *the Pliocene intensification of Northern Hemisphere glaciations*.
49 441 *Paleoceanography*, 2011. **26**.
50 442 9. Lisiecki, L.E. and M.E. Raymo, *A Pliocene-Pleistocene stack of 57 globally*
51 443 *distributed benthic delta O-18 records (vol 20, art no PA1003, 2005)*.
52 444 *Paleoceanography*, 2005. **20**(2).
53 445 10. Siegenthaler, U., et al., *Stable Carbon Cycle-Climate Relationship During the*
54 446 *Late Pleistocene*. *Science*, 2005. **310**(5752): p. 1313-1317.
55
56
57
58
59
60

- 1
2
3 447 11. Petit, J.R., et al., *Climate and atmospheric history of the past 420,000 years*
4 448 *from the Vostok ice core, Antarctica*. Nature, 1999. **399**(6735): p. 429-436.
5 449 12. Luthi, D., et al., *High-resolution carbon dioxide concentration record*
6 450 *650,000-800,000 years before present*. Nature, 2008. **453**(7193): p. 379-382.
7 451 13. Popp, B.N., et al., *Effect of phytoplankton cell geometry on carbon isotopic*
8 452 *fractionation*. Geochimica Et Cosmochimica Acta, 1998. **62**(1): p. 69-77.
9 453 14. Riebesell, U., et al., *The effects of varying CO₂ concentration on lipid*
10 454 *composition and carbon isotope fractionation in Emiliania huxleyi*.
11 455 Geochimica Et Cosmochimica Acta, 2000. **64**(24): p. 4179-4192.
12 456 15. Laws, E.A., et al., *Dependence of Phytoplankton Carbon Isotopic*
13 457 *Composition on Growth-Rate and [CO₂](Aq) - Theoretical Considerations*
14 458 *and Experimental Results*. Geochimica Et Cosmochimica Acta, 1995. **59**(6): p.
15 459 1131-1138.
16 460 16. Bidigare, R.R., et al., *Consistent fractionation of C-13 in nature and in the*
17 461 *laboratory: Growth-rate effects in some haptophyte algae*. Global
18 462 Biogeochemical Cycles, 1997. **11**(2): p. 279-292.
19 463 17. Laws, E.A., R.R. Bidigare, and B.N. Popp, *Effect of growth rate and CO(2)*
20 464 *concentration on carbon isotopic fractionation by the marine diatom*
21 465 *Phaeodactylum tricornutum*. Limnology and Oceanography, 1997. **42**(7): p.
22 466 1552-1560.
23 467 18. Bidigare, R.R., et al., *Iron-stimulated changes in C-13 fractionation and*
24 468 *export by equatorial Pacific phytoplankton: Toward a paleogrowth rate proxy*.
25 469 Paleooceanography, 1999. **14**(5): p. 589-595.
26 470 19. Hayes, J.M., et al., *Compound-Specific Isotopic Analyses - a Novel Tool for*
27 471 *Reconstruction of Ancient Biogeochemical Processes*. Organic Geochemistry,
28 472 1990. **16**(4-6): p. 1115-1128.
29 473 20. Marlowe, I.T., et al., *Long-Chain Alkenones and Alkyl Alkenoates and the*
30 474 *Fossil Coccolith Record of Marine-Sediments*. Chemical Geology, 1990. **88**(3-
31 475 4): p. 349-375.
32 476 21. Romanek, C.S., E.L. Grossman, and J.W. Morse, *Carbon Isotopic*
33 477 *Fractionation in Synthetic Aragonite and Calcite - Effects of Temperature and*
34 478 *Precipitation Rate*. Geochimica Et Cosmochimica Acta, 1992. **56**(1): p. 419-
35 479 430.
36 480 22. Mook, W.G., Bommerso.Jc, and Staverma.Wh, *Carbon Isotope Fractionation*
37 481 *between Dissolved Bicarbonate and Gaseous Carbon-Dioxide*. Earth and
38 482 Planetary Science Letters, 1974. **22**(2): p. 169-176.
39 483 23. Pagani, M., et al., *Marked decline in atmospheric carbon dioxide*
40 484 *concentrations during the Paleogene*. Science, 2005. **309**(5734): p. 600-603.
41 485 24. Weiss, R.F., *The solubility of nitrogen, oxygen and argon in water and*
42 486 *seawater*. Deep Sea Research and Oceanographic Abstracts, 1970. **17**(4): p.
43 487 721-735.
44 488 25. Weiss, R.F., *Carbon dioxide in water and seawater: the solubility of a non-*
45 489 *ideal gas*. Marine Chemistry, 1974. **2**(3): p. 203-215.
46 490 26. Pagani, M., M.A. Arthur, and K.H. Freeman, *Miocene evolution of*
47 491 *atmospheric carbon dioxide*. Paleooceanography, 1999. **14**(3): p. 273-292.
48 492 27. Pagani, M., et al., *The Role of Carbon Dioxide During the Onset of Antarctic*
49 493 *Glaciation*. Science, 2011. **334**(6060): p. 1261-1264.
50 494 28. Bijl, P.K., et al., *Transient Middle Eocene Atmospheric CO(2) and*
51 495 *Temperature Variations*. Science, 2010. **330**(6005): p. 819-821.
52
53
54
55
56
57
58
59
60

- 1
2
3 496 29. Takahashi, T., et al., *Climatological mean and decadal change in surface*
4 497 *ocean pCO₂, and net sea-air CO₂ flux over the global oceans (vol 56, pg*
5 498 *554, 2009)*. Deep-Sea Research Part I-Oceanographic Research Papers, 2009.
6 499 **56**(11): p. 2075-2076.
7 500 30. Brassell, S.C., et al., *Molecular Stratigraphy - a New Tool for Climatic*
8 501 *Assessment*. Nature, 1986. **320**(6058): p. 129-133.
9 502 31. Prah, F.G. and S.G. Wakeham, *Calibration of Unsaturation Patterns in Long-*
10 503 *Chain Ketone Compositions for Paleotemperature Assessment*. Nature, 1987.
11 504 **330**(6146): p. 367-369.
12 505 32. Muller, P.J., et al., *Calibration of the alkenone paleotemperature index U-*
13 506 *37(K') based on core-tops from the eastern South Atlantic and the global*
14 507 *ocean (60 degrees N-60 degrees S)*. Geochimica Et Cosmochimica Acta,
15 508 1998. **62**(10): p. 1757-1772.
16 509 33. Conte, M.H., et al., *Global temperature calibration of the alkenone*
17 510 *unsaturation index (U(37)(K')) in surface waters and comparison with*
18 511 *surface sediments*. Geochemistry Geophysics Geosystems, 2006. **7**.
19 512 34. Groeneveld, J., *Effect of the Pliocene closure of the Panamanian Gateway on*
20 513 *Caribbean and east Pacific sea surface temperatures and salinities by*
21 514 *applying combined Mg/Ca and $\delta^{18}O$ measurements (5.6-2.2Ma)*, 2005,
22 515 University of Kiel: Kiel. p. 165.
23 516 35. Locarnini, R.A., et al., *World Ocean Atlas 2009, Volume 1: Temperature*.
24 517 NOAA Atlas NESDIS 68, ed. S. Levitus 2010, Washington, D.C.: U.S
25 518 Government Printing Office.
26 519 36. Barnola, J.M., et al., *Vostok ice core provides 160,000-year record of*
27 520 *atmospheric CO₂*. Nature, 1987. **329**(6138): p. 408-414.
28 521 37. Kameo, K. and T.J. Bralower, *Neogene calcareous nannofossil*
29 522 *biostratigraphy of Site 998, 999 and 1000, Caribbean Sea*, in *Proceedings of*
30 523 *the Ocean Drilling Program, Scientific Results*, R.M. Leckie, et al., Editors.
31 524 2000, Ocean Drilling Program: College Station, TX. p. 3-17.
32 525 38. Herrmann, S. and H.R. Thierstein, *Cenozoic coccolith size changes-*
33 526 *Evolutionary and/or ecological controls?* Palaeogeography Palaeoclimatology
34 527 Palaeoecology, 2012. **333**: p. 92-106.
35 528 39. Henderiks, J. and M. Pagani, *Refining ancient carbon dioxide estimates:*
36 529 *Significance of coccolithophore cell size for alkenone-based pCO₂ records*.
37 530 Paleoceanography, 2007. **22**(3).
38 531 40. Plancq, J., et al., *Alkenone producers during late Oligocene-early Miocene*
39 532 *revisited*. Paleoceanography, 2012. **27**.
40 533 41. O'dea, A., et al., *Environmental change preceded Caribbean extinction by 2*
41 534 *million years*. Proceedings of the National Academy of Sciences of the United
42 535 States of America, 2007. **104**(13): p. 5501-5506.
43 536 42. Haug, G.H. and R. Tiedemann, *Effect of the formation of the Isthmus of*
44 537 *Panama on Atlantic Ocean thermohaline circulation*. Nature, 1998.
45 538 **393**(6686): p. 673-676.
46 539 43. Party, S.S., *Site 999*, in *Proceeding of the Ocean Drilling Program. Initial*
47 540 *Reports*, R. Haraldur Sigurdsson, et al., Editors. 1997, Ocean Drilling
48 541 Program: College Station, TX. p. 131-230.
49 542 44. Laws, E.A., et al., *Controls on the molecular distribution and carbon isotopic*
50 543 *composition of alkenones in certain haptophyte algae*. Geochemistry
51 544 Geochemistry Geophysics Geosystems, 2001. **2**.

- 1
2
3 545 45. Garcia, H.E., et al., *World Ocean Atlas 2009, Volume 4: Nutrients (phosphate,*
4 546 *nitrate, silicate)*. NOAA Atlas NESDIS 71, ed. S. Levitus 2010, Washington,
5 547 D.C.: U.S Government Printing Office.
6 548 46. Nurnberg, D., J. Bijma, and C. Hemleben, *Assessing the reliability of*
7 549 *magnesium in foraminiferal calcite as a proxy for water mass temperatures.*
8 550 *Geochimica Et Cosmochimica Acta*, 1996. **60**(5): p. 803-814.
9 551 47. Dekens, P.S., et al., *A 5 million year comparison of Mg/Ca and alkenone*
10 552 *paleothermometers.* *Geochemistry Geophysics Geosystems*, 2008. **9**.
11 553 48. Anand, P., H. Elderfield, and M.H. Conte, *Calibration of Mg/Ca thermometry*
12 554 *in planktonic foraminifera from a sediment trap time series.*
13 555 *Paleoceanography*, 2003. **18**(2).
14 556 49. Fantle, M.S. and D.J. DePaolo, *Sr isotopes and pore fluid chemistry in*
15 557 *carbonate sediment of the Ontong Java Plateau: Calcite recrystallization*
16 558 *rates and evidence for a rapid rise in seawater Mg over the last 10 million*
17 559 *years.* *Geochimica et Cosmochimica Acta*, 2006. **70**(15): p. 3883-3904.
18 560 50. Honisch, B., et al., *Atmospheric Carbon Dioxide Concentration Across the*
19 561 *Mid-Pleistocene Transition.* *Science*, 2009. **324**(5934): p. 1551-1554.
20 562
21 563
22
23
24
25
26
27
28
29
30
31
32
33
34
35
36
37
38
39
40
41
42
43
44
45
46
47
48
49
50
51
52
53
54
55
56
57
58
59
60

564

565 **Figure Captions**

566 **Figure 1a.** ε_p values (filled square symbols and fine black line) are shown with the
567 epibenthic foraminiferal oxygen isotope record for the site (Grey/heavy solid line; [42])
568 for comparison. For ε_p the plotted uncertainty envelopes represent maximum and
569 minimum estimates based on 2σ extremes of the $\delta^{13}\text{C}_{37:2}$ measurement (dashed line)
570 and a full monte carlo propagation of associated uncertainties (dotted line; see main
571 text for details). **b.** *G. ruber* (open diamonds) and alkenone $\delta^{13}\text{C}$ values (filled
572 circles); error bars are 2σ analytical errors based on replicate measurements.

573 **Figure 2a.** $p\text{CO}_2$ reconstruction based on our new high resolution $\delta^{13}\text{C}_{37:2}$ records
574 (filled squares and line); as in Figure 1, the dashed line shows an uncertainty envelope
575 representing minimum and maximum estimates based on 2σ extremes of the $\delta^{13}\text{C}_{37:2}$
576 measurement (dashed line) and a full monte carlo propagation of associated
577 uncertainties (dotted line; see main text for details). **b.** Sea surface temperature
578 estimates based on the alkenone unsaturation index. Calibration and measurement
579 uncertainties are approximately 2°C and are omitted for clarity. **c.** Benthic
580 foraminiferal oxygen isotope stack LR04 (Grey/heavy solid line; [9]) for comparison.

581 **Figure 3** Selected records of $p\text{CO}_2$ and climate from the Pliocene to present. **a.**
582 Alkenone-based $p\text{CO}_2$ records from Seki et al. [7] corrected for cell geometry (dashed
583 line; minimum and maximum estimates) and uncorrected (purple filled squares and
584 line; minimum and maximum estimates) and Pagani et al. [6] shown here as their
585 reconstructed ' $\text{CO}_{2\text{slope}}$ ' (from top to bottom: from ODP sites 1012 [khaki heavy line];
586 1208 [green heavy line]; 982 [cyan heavy line]; 1012 with an alternative nutrient
587 scenario [heavy dashed line]; and 806 [lilac heavy line]. Our record is shown as open

1
2
3 588 squares and line with the error envelope from the monte carlo model (see text). **b.**
4
5 589 $\delta^{11}\text{B}$ -based $p\text{CO}_2$ records from Seki et al. [7] calculated using modelled $[\text{CO}_3^{2-}]$ (blue
6
7 590 filled diamonds) and assuming modern total alkalinity (TA; red filled circles). Error
8
9 591 bars are ± 25 ppm and the error envelope is based on varying TA by $\pm 5\%$. The records
10
11 592 of Bartoli et al. [8] are shown in grey, (open grey circles and line, with 2σ uncertainty
12
13 593 envelope) along with that of Hönisch et al. [50] (filled grey circles and line, , with 2σ
14
15 594 uncertainty envelope). Also shown is the Antarctic ice core record of $p\text{CO}_2$ over the
16
17 595 last 800 Kyr for comparison ([12] and references therein). **c.** Benthic foraminiferal
18
19 596 oxygen isotope stack LR04 (Grey/heavy solid line; [9]) for comparison (Online
20
21 597 version in colour.)
22
23
24
25

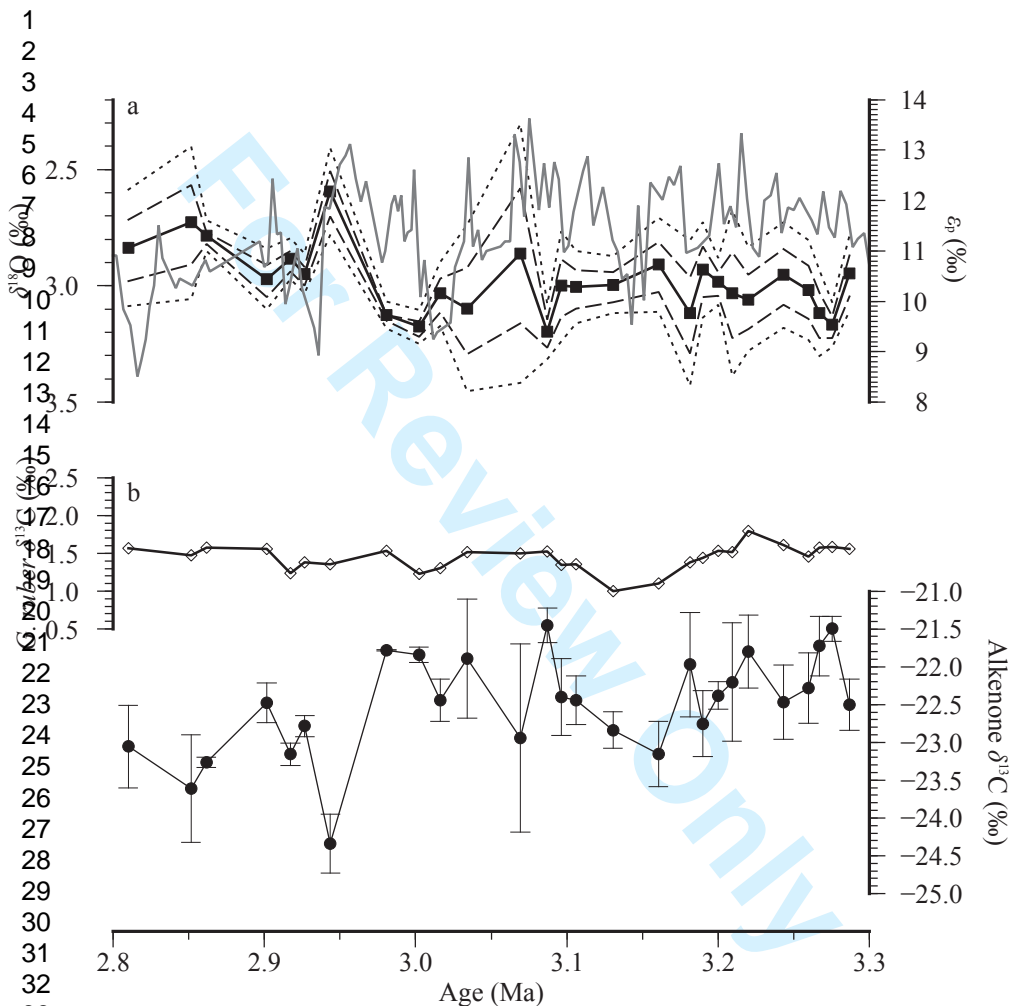
26 598 **Figure 4** Pliocene $p\text{CO}_2$ records from ODP Site 999. **a** Alkenone-based $p\text{CO}_2$ records
27
28 599 from Seki et al. [7] corrected for cell geometry (dashed line; minimum and maximum
29
30 600 estimates) and uncorrected (purple filled squares and line; minimum and maximum
31
32 601 estimates) and our new higher resolution record (filled squares and line); the dashed
33
34 602 line shows an uncertainty envelope representing minimum and maximum estimates
35
36 603 based on 2σ extremes of the $\delta^{13}\text{C}_{37:2}$ measurement (dashed line) and a full monte carlo
37
38 604 propagation of associated uncertainties (dotted line; see main text for details). **b** $\delta^{11}\text{B}$ -
39
40 605 based $p\text{CO}_2$ records from Seki et al. [7] calculated using modelled $[\text{CO}_3^{2-}]$ (blue filled
41
42 606 diamonds) and assuming modern total alkalinity (TA; red filled circles). Error bars are
43
44 607 ± 25 ppm and the error envelope is based on varying TA by $\pm 5\%$. The record of
45
46 608 Bartoli et al. [8] is shown as grey open circles and line with 2σ uncertainty envelope
47
48 609 (grey lines). **c.** Benthic foraminiferal oxygen isotope stack LR04 (Grey/heavy solid
49
50 610 line; [9]) for comparison (Online version in colour.)
51
52
53
54
55
56
57
58
59
60

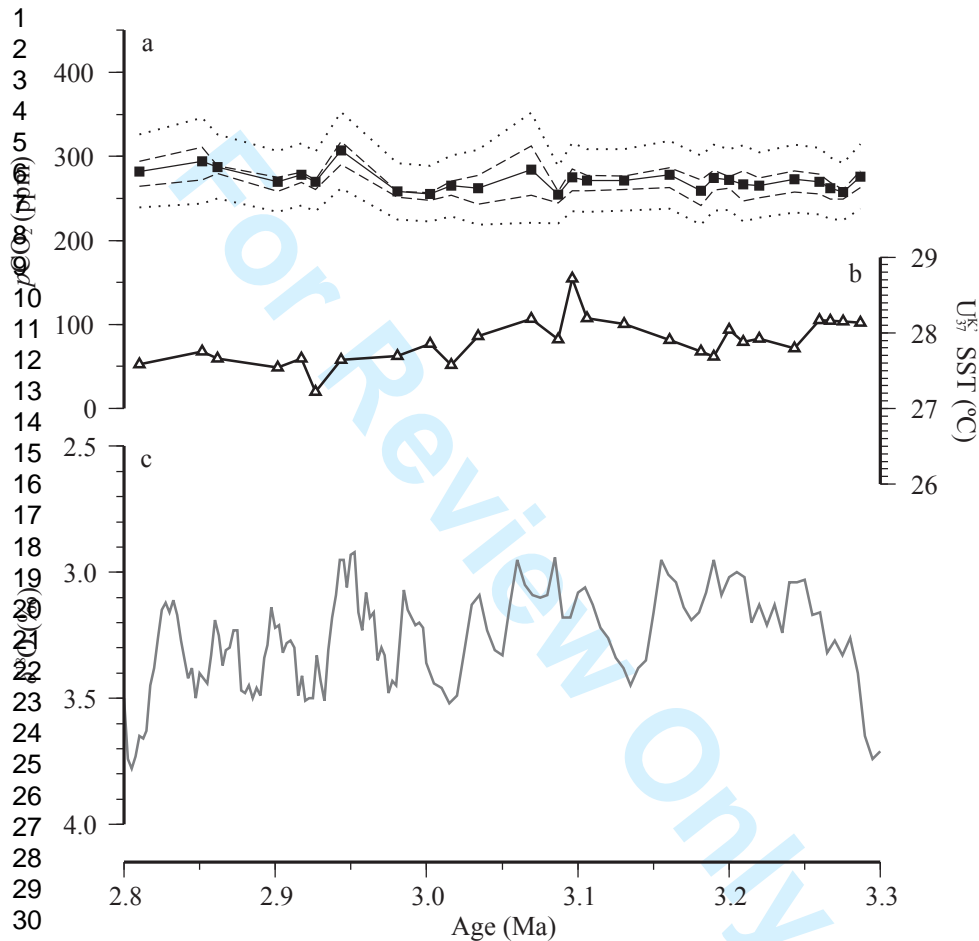
1
2
3 611 **Figure 5** The effect of the coccolith length ($L_{\text{coccolith}}$) correction on reconstructed
4
5 612 $p\text{CO}_2$. Lines represent the correction applied at different sea surface temperatures at 3
6
7 613 $^{\circ}\text{C}$ intervals (as labelled). White circles represent the uncorrected values (where the
8
9 614 coccolith length equals that of modern cultured coccolithophores). These were
10
11 615 calculated based on representative values of $\delta^{13}\text{C}_{37:2} = -20 \text{ ‰}$ and $\delta^{13}\text{C}_{\text{cc}} = 2 \text{ ‰}$, $[\text{PO}_4^{3-}] = 0.25 \mu\text{M}$
12
13 616 and $S = 35 \text{ psu}$.

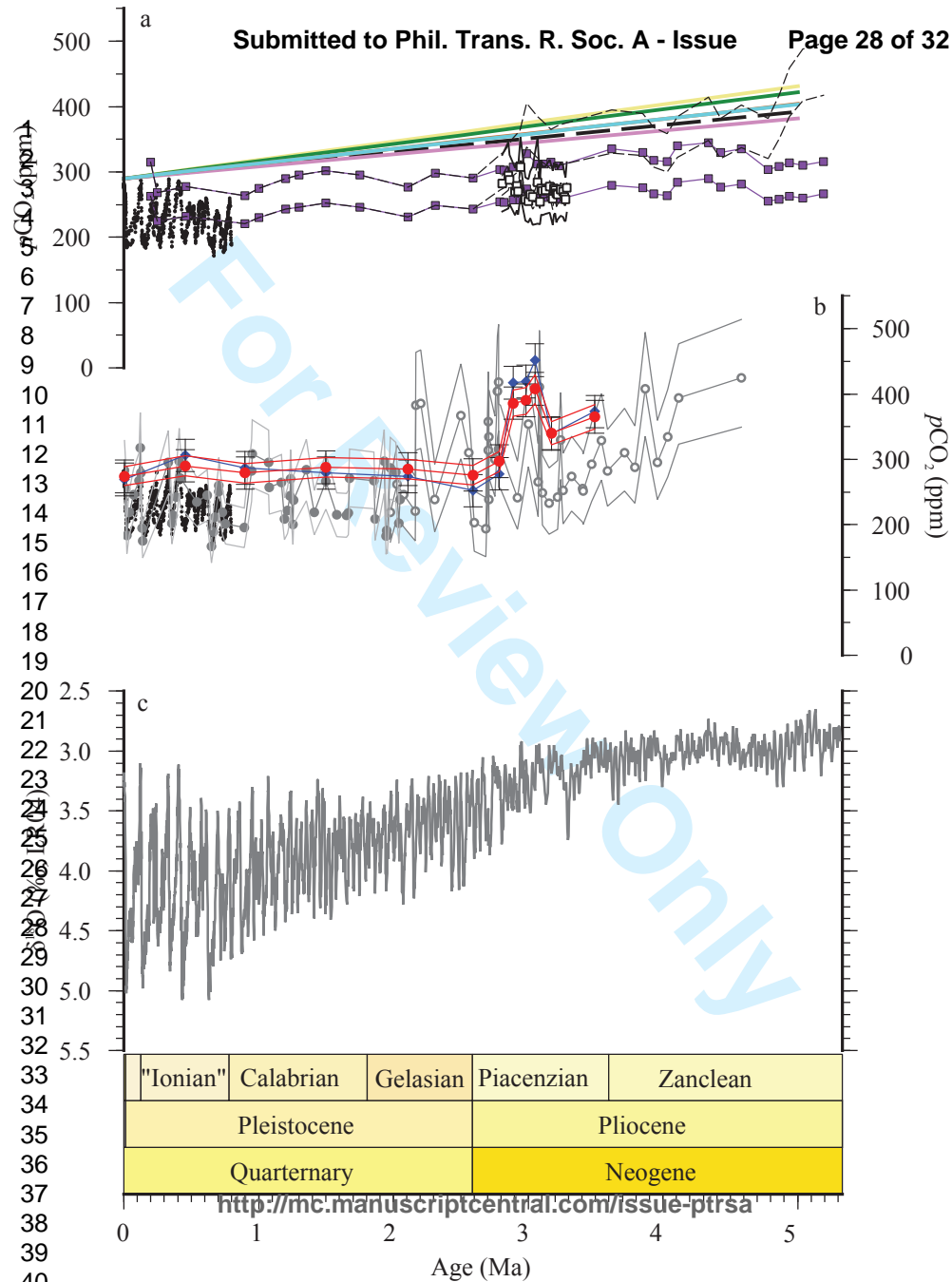
14
15
16
17 617 **Figure 6** Phosphate concentrations are closely correlated with apparent 'b' term, most
18
19 618 likely due to a linkage to growth rate. Our favoured assumption uses the modern day
20
21 619 concentration for the site ($0.2 \mu\text{M}$; black filled squares and line) with minimum and
22
23 620 maximum estimates based on 2σ extremes of the $\delta^{13}\text{C}_{37:2}$ measurement (dashed line)
24
25 621 and a full monte carlo propagation of associated uncertainties (which includes a ± 0.1
26
27 622 μM on $[\text{PO}_4^{3-}]$; dotted line; see main text for details). We also include reconstructions
28
29 623 with $[\text{PO}_4^{3-}]$ representative of an oligotrophic site ($0.05 \mu\text{M}$; open squares), a high
30
31 624 nutrient area similar to the eastern equatorial Pacific ($0.6 \mu\text{M}$; open triangles) and an
32
33 625 extreme case representative of an active upwelling region ($0.9 \mu\text{M}$; open circles)[45].
34
35 626 The appropriate 'b' term according to the relationship of Pagani et al. [6] is shown for
36
37 627 each reconstruction.

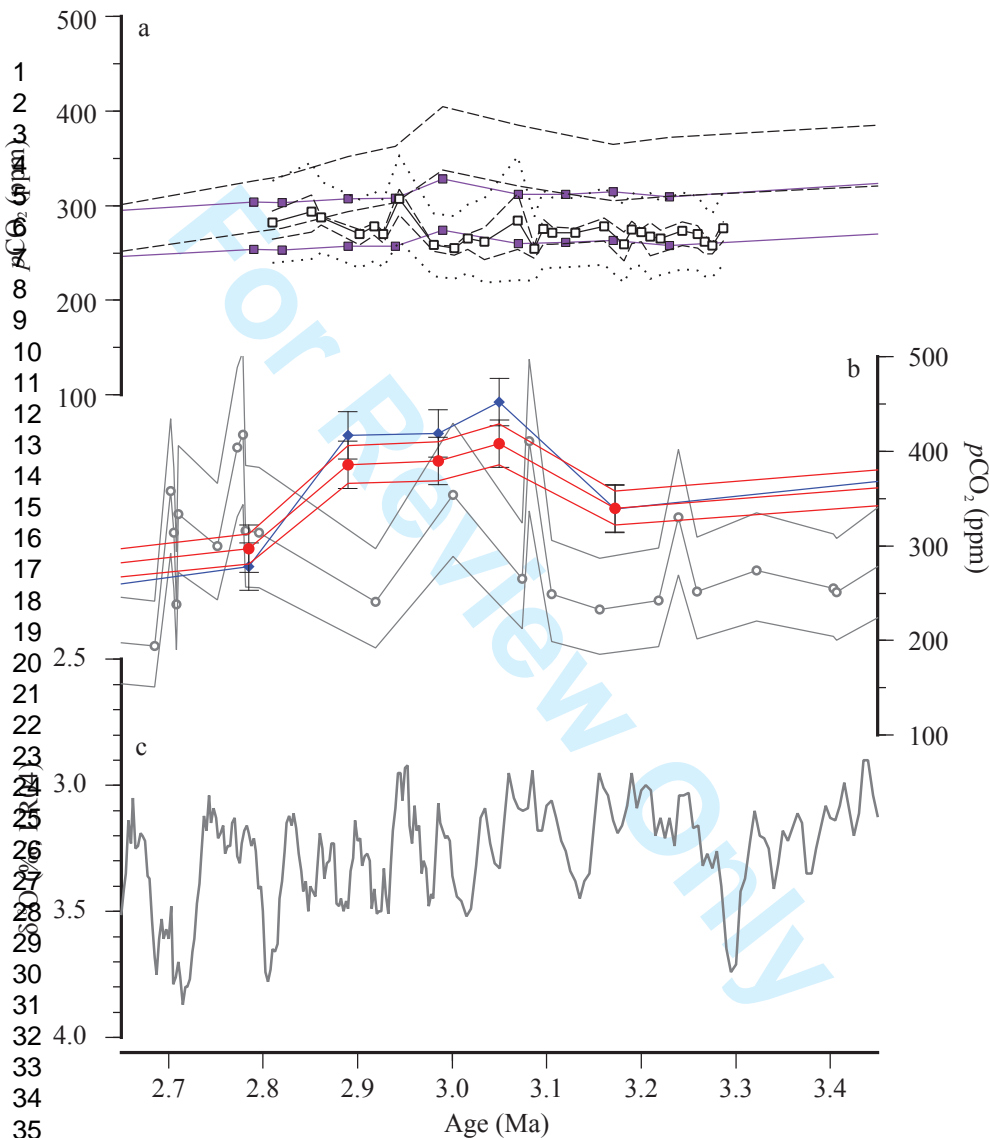
38
39
40
41
42 628 **Figure 7** The relationship between ε_p and alkenone $\delta^{13}\text{C}$ (**a**); $[\text{CO}_{2(\text{aq})}]$ and $p\text{CO}_2$ (**b**);
43
44 629 ε_p and $p\text{CO}_2$ (**c**); and alkenone and $\delta^{13}\text{C}$ (**d**) are all affected by SST. Lines are
45
46 630 calculated at varied SST at $3 \text{ }^{\circ}\text{C}$ intervals (as labelled), and were calculated based on
47
48 631 representative starting values of $\delta^{13}\text{C}_{37:2} = -20 \text{ ‰}$; $\delta^{13}\text{C}_{\text{cc}} = 2 \text{ ‰}$. $[\text{PO}_4^{3-}] = 0.25 \mu\text{M}$,
49
50 632 $S = 35 \text{ psu}$.

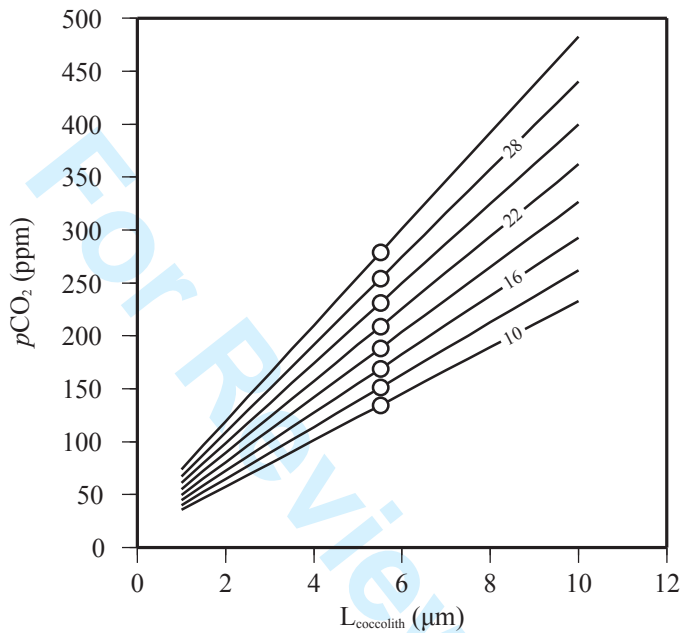
51
52
53
54
55 633 **Short title:** *Stable Pliocene $p\text{CO}_2$*











1

2

3

4

5

6

7

8

9

10

11

12

13

14

15

16

17

18

19

20

21

22

23

24

25

26

27

28

29

30

31

32

33

34

35

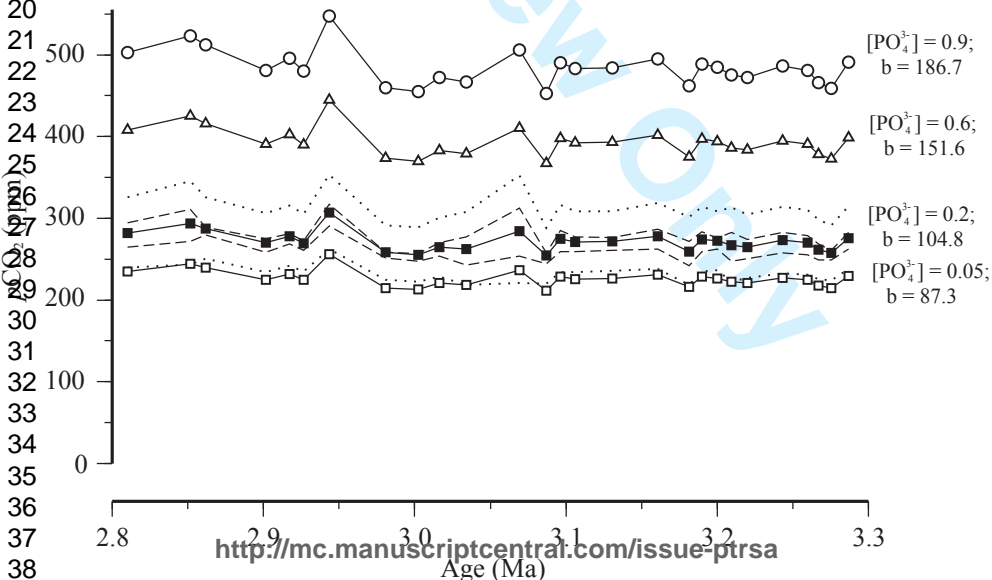
36

37

38

39

40



<http://mc.manuscriptcentral.com/issue-ptrsa>
Age (Ma)

